Title
Ice retreat in Wilkes Basin of East Antarctica during a warm interglacial.

Journal
Nature, 583(7817)

ISSN
0028-0836

Authors
Blackburn, T
Edwards, GH
Tulaczyk, S
et al.

Publication Date
2020-07-01

DOI
10.1038/s41586-020-2484-5

Peer reviewed

Ice retreat in Wilkes Basin of East Antarctica during a warm interglacial

T. Blackburn[1*], G.H. Edwards[1], S. Tulaczyk[1], M. Scudder[1], G. Piccione[1], B. Hallet[2], N. McLean[3], J.C. Zachos[1], B. Cheney[1], J.T. Babbe[1]

[1]Earth and Planetary Science, University of California, Santa Cruz, Santa Cruz, CA USA

[2]Quaternary Research Center, University of Washington, Seattle, WA, USA

[3]Department of Geology, University of Kansas, Lawrence, KS 66045, USA

*Correspondence to: terryb@ucsc.edu

Efforts to improve sea level forecasting on a warming planet have focused on determining the temperature, sea level and extent of polar ice sheets during Earth's past interglacial warm periods[1-3]. At ~400 thousand years before present, during the interglacial period known as Marine Isotopic Stage 11 (MIS 11), the Earth, globally was 1-2°C warmer[2] and sea level was 6-13m[1,3] higher. Sea level estimates in excess of ~10m, however, have been discounted as these require contribution from the East Antarctic Ice Sheet[3], which has been argued to have remained stable at MIS 11 and for millions of years prior[4,5]. Here, we show how the evolution of ^{234}U enrichment within subglacial waters of East Antarctica records the ice sheet response to MIS 11 warming. Within the Wilkes Basin, subglacial chemical precipitates of opal and calcite record the accumulation of ^{234}U, the product of rock-water contact within an isolated subglacial reservoir, up to 20 times higher than marine waters. The timescales of ^{234}U enrichment place the inception of this reservoir to MIS 11. Informed by the observed ^{234}U cycling in the Laurentide ice sheet, where ^{234}U accumulated during periods of ice stability[6] and was purged in response to deglaciation[7], we interpret our East Antarctic dataset to record ice loss within the Wilkes Basin at MIS 11. The ^{234}U ingrowth within the Wilkes Basin is shared by the McMurdo Dry Valley brines[8-10], supporting[11] brine origination beneath the adjacent East Antarctic ice sheet. The requirement that brine salts[10] and bacteria[12] are from marine waters implies that MIS 11 ice loss was coupled with marine flooding. Collectively these data indicate that during one of the warmest Pleistocene interglacials, the ice sheet margin at the Wilkes Basin retreated to the proximity of the precipitate location, ~700km inland from the current position, which assuming current ice volumes, would contribute ~3-4m[13] to global seas.

Introduction

Large uncertainties in reconstructions of sea level highstands during Earth's past warm interglacial periods, as well as in the predictions of future sea level rise, result in part, from the poorly constrained climate sensitivity of the East Antarctic Ice Sheet (EAIS). The EAIS is the world's largest freshwater reservoir and ice loss in response to a warming climate is expected to be focused on the low elevation basins most susceptible to grounding line retreat, including the Wilkes, Pensacola and Aurora Basins[14], which can collectively contribute 8-10 m in sea level rise[15] (Fig. 1). Yet an idea that has prevailed for decades, argues that the EAIS has remained stable on million-year timescales[4,5]. The apparent stability of East Antarctica is inferred primarily from the preservation of ancient glacial features, slow erosion and a lack of evidence for major melting within the Transantarctic Mountains[4,5], the polar desert range that borders the EAIS (Fig. 1). And while this result was initially supported by ice sheet models that required unrealistic warming (>10 °C) to yield ice loss[16], recent models that incorporate ice-ocean interactions do predict an East Antarctic response to modest warming within low elevation basins, including the Wilkes Basin while preserving ice in the Transantarctics[13,14]. The susceptibility of the marine basins to deglaciation has gained support from observations gathered from Pleistocene sediment cores collected offshore of the Wilkes Basin[17]. These data reveal oscillations in the provenance of detrital sediment that have been interpreted to reflect a shift from coastal to on-continent erosion driven by Wilkes Basin ice loss during interglacial periods MIS 5, 9 and 11 that was greater than the ice loss observed in the Holocene. Despite these theoretical advances and observations that have shifted scientific views towards a more dynamic EAIS, neither the computational models nor offshore sedimentary records are capable of determining both the timing *and* magnitude of EAIS deglaciation during Pleistocene interglacials. These past interglacial warm periods are characterized by global warming of 1-2 °C above preindustrial temperatures, a significant warming increase that is analogous to projected near future climate[1]. Any additional means for recognizing the timing and magnitude of past ice loss events for East Antarctica in response to warming, may clarify the height of sea level highstands in both the past and future.

Such additional methods for documenting ice sheet collapse have recently been developed by Chen and others[7] who showed that the collapse of the Laurentide ice sheet at 15-20 thousand years ago (ka) was associated with a transient 3 ‰ increase in the $\delta^{234}U$ ($\delta^{234}U = [(^{234}\mathrm{U}/^{238}\mathrm{U})_{\mathrm{AR}} - 1]\cdot 1000$) composition of Atlantic waters relative to modern seawater. Aqueous enrichment in ^{234}U above secular equilibrium ($\delta^{234}U = 0$ ‰) reflects rock-water interaction[18] and in glacial systems may be attributed to the recoil-injection of ^{234}U into basal ice and subglacial waters incurred during the α-decay of parent ^{238}U housed within debris-laden basal ice and subglacial sediments (Fig. 2, inset). From the change in ocean water compositions, Chen and others[7] inferred that a reservoir strongly enriched in ^{234}U within the Laurentide ice sheet was flushed rapidly into the ocean during early phases of the last glacial termination. They pointed to the brines of the McMurdo Dry Valleys, Antarctica, which currently exhibit $\delta^{234}U$ compositions greater than 3000 ‰[8,10], as a possible analog to the Laurentide ^{234}U-enriched reservoir.

Results

Here, we report results from a new Antarctic archive of $\delta^{234}U$ compositions: chemical precipitates formed in subglacial aquatic environments beneath the EAIS. These aqueous chemical precipitates form as a byproduct of subglacial freezing, a process that consumes subglacial waters, concentrating solutes to the point of calcite [19,20] or amorphous silica/opal[21,22] precipitation. The oxygen compositions of Antarctic calcite precipitates are among the most ^{18}O depleted compositions on Earth[20,23,24], which confirms their precipitation from Antarctic subglacial waters[23]. Precipitates sampled from either deglaciated bedrock surfaces[23,24] or from exposed sections of basal ice/moraines[20,25], place the location of precipitate formation beneath the ice. Because they can be dated by ^{234}U-^{230}Th methods (see methods), these precipitates record the $\delta^{234}U$ of subglacial waters at the time of sample precipitation ($\delta^{234}U_i$) and collectively reveal that ^{234}U enrichment is not limited to the waters of the McMurdo Dry Valleys alone, but rather, is observed to be both geographically and temporally ubiquitous in the aquatic environments of East Antarctica (Fig. 1).

Figure 1 shows the distribution of both new (Table 1*)* and existing[24-26] U-series data for five EAIS precipitate locations, four of which border the EAIS along the Transantarctic Mountains within the Pensacola and Wilkes Basin and a fifth within the Aurora basin. Precipitates from each of these locations exhibit $\delta^{234}U_i$ compositions well in excess of secular equilibrium and marine compositions ($\delta^{234}U$ = 145 ‰ [27], Fig. 1). These observations imply that subglacial waters are the source and cause of change in marine $\delta^{234}U$[7] at 15-20 ka and inform us that basal waters from the Laurentide ice sheet were flushed in advance of large-scale deglaciation. A comparison between the ^{234}U-^{230}Th date and the $\delta^{234}U_i$ for EAIS precipitates yields an apparent shared history for this continent-scale compilation that is characterized by ^{234}U accumulation with $\delta^{234}U_i$ increasing by >2000 ‰ over the last ~300 ka (Fig. 3). Part of this long-term archive of ^{234}U accumulation is recorded in a singular geographic location by a subglacial precipitate sample from Elephant Moraine (PRR50489). This centimeter-thick sample of layered opal and calcite has been dated at multiple horizons, revealing ^{234}U-^{230}Th dates that span from 265 to 150 ka and record changes of $\delta^{234}U_i$ within the subglacial waters of the Wilkes subglacial basin of >700 ‰ (Fig 3). An additional sample from Elephant Moraine (PRR39222), also exhibits variations in $\delta^{234}U$ with stratigraphic position. Though low U/Th for PRR39222 inhibits a reliable age determination, the measured $\delta^{234}U$ values, uncorrected for ^{234}U decay, are ~40-140 ‰ and correlate with stratigraphic position (top = higher $\delta^{234}U$, Table 1). With the formation time unknown, we can instead model the $\delta^{234}U_i$ values for 0-450 ka formation for both the sample top and bottom (Fig. 3, purple curves). If we assume sample precipitation rates (0.5 – 5 mm/ka) similar to Antarctic calcite dated by U-Th methods (e.g. PRR50489) we can define a formation duration for PRR39222 (45 mm) of ~10-90 ka. Assuming these durations, along with the requirement that the sample bottom and top intersects the purple curves shown in figure 3, permits definition of possible $\delta^{234}U_i$ ingrowth histories (black arrows, Fig. 3). We find that possible ingrowth histories are congruent with the shared $\delta^{234}U_i$ ingrowth history for the region if this sample formed at ~400 ka (Extended data Fig. 3) but incongruent at earlier formation times (Extended data Fig. 3). And while uncertainty on the age of PRR39222 remains, the occurrence of low $\delta^{234}U$ (<500 ‰) in subglacial fluids is apparently rare (Fig. 3), having been identified in this region only in samples older than ~300 ka (with the exception of a single outlier in the Taylor Valley dataset). This suggests that PRR39222 records the ingrowth of ^{234}U within Wilkes Basin waters at ~300-400 ka.

As introduced above, ^{234}U enrichment has been recorded in waters of the McMurdo Dry Valleys (MDV). The MDV are the largest ice-free area of Antarctica, where land terminating glaciers permit subglacial brines to emanate onto the surface or into proglacial lakes[11]. The source of MDV fluids has been extensively studied: the geochemistry[10], isotopic composition[28] and bacterial ecosystems[12] all point to origination from a marine flooding event that occurred prior to isolation of fluids from the atmosphere on timescales greater than 200 ka[29,30] (see methods for further discussion). Citing observations of ancient preserved features and slow erosion within the Transantarctic mountains[4,5], the timing of the marine incursion associated with MDV brines has often been relegated to occurring millions of years ago in the warmer Miocene climate[10,12]. Modern MDV brines and surface lakes found in both Taylor and Wright valley, however, are observed to share characteristics with fluids beneath the EAIS: they are currently strongly enriched in ^{234}U (Fig. 1, $\delta^{234}U$ >3000 ‰) [8,10]. Carbonates that formed within past proglacial lakes of Taylor Valley also record elevated $\delta^{234}U$ values[9], suggesting that these paleolakes, like modern Lake Bonney[11], were also fed by subglacial waters. Similar to the subglacial precipitates in the EAIS, we note that the existing data for these MDV lake carbonates document an increase in $\delta^{234}U_i$ over the last ~300 thousand years (Fig. 3a). This coevolution of $\delta^{234}U$ in MDV and EAIS fluids supports the view that MDV brines are much younger than the Miocene and have been sourced from subglacial EAIS fluids within the Wilkes Basin that have been cryoconcentrated in transit by subglacial freezing[11].

The accumulation to high values (>3000 ‰) and the evolution of $\delta^{234}U_i$ with time as recorded by EAIS precipitates, MDV lake carbonates and modern fluids both match the model predictions of ^{234}U ingrowth by direct injection into fluids during the decay of ^{238}U housed within subglacial sediments (Fig. 2 and supplementary information (SI)). Collectively, these data point to a subglacial water reservoir starting with low $\delta^{234}U$ compositions that have increased by ^{234}U recoil ejection from sediments but has not yet reached a steady state $\delta^{234}U$ composition, which is attained after >1 million years of rock-water contact (Fig. 2). To place an estimate on the duration of rock-water contact, we employ a model that simulates ^{234}U ingrowth histories from α-recoil and explores two key variables: the onset time and the steady state $\delta^{234}U$ ($\delta^{234}U_{SS}$) (see SI). A number of physical variables influence the rate of ^{234}U ingrowth and $\delta^{234}U_{SS}$, including sediment grain size, uranium content and porosity (Fig. 2). For our purposes of estimating the timing of reservoir inception, we need not uniquely determine any of these reservoir traits which, given their occurrence beneath the EAIS, are poorly known. Rather, we can explore extreme ranges of all variables via their net effect on $\delta^{234}U_{SS}$ and identify, using a maximum likelihood test, the model ingrowth histories that best match the measured data. However, it is expected that the physical traits controlling ^{234}U accumulation differ from one subglacial reservoir to the next (Fig. 2). For example, the ~2000 ‰ range in $\delta^{234}U$ observed between modern waters and young (<25 ka) precipitates from across East Antarctica likely reflects differences in the sediment characteristics between these geographically and geologically distinct regions (Fig. 3). This heterogeneity does not apply to sample PRR50489, a centimeter-thick sample that provides a >100 ka record of ^{234}U accumulation beneath the ice in a singular location. Using a maximum likelihood test, we compare the measured results for PRR50489 with model simulations of ^{234}U ingrowth for a range of reservoir isolation times (100-800 ka), initial $\delta^{234}U$ for the subglacial reservoir (0-1500 ‰) and $\delta^{234}U_{SS}$ (2000-9000 ‰). The uncertainty in the timing of reservoir isolation is dominated by the possible range of initial $\delta^{234}U$ compositions for the reservoir. Assuming values as low as those observed in sample PRR39222 or marine compositions (145 ‰), best-fit paths correspond to reservoir inception times of 435 +20/-25 ka (95% confidence interval, χ_v^2=3.9) (Fig. 3b,c). If the reservoir were initially enriched in ^{234}U, perhaps up to 500 ‰ as in the oldest carbonates found in Taylor Valley the best fit path is shifted with an inception time of 390 +25/-15 ka (95% confidence interval, χ_v^2=3.9) (Fig. 3c). Thus, even assuming a range of initial $\delta^{234}U$ compositions that lie between sample PRR39222 and the oldest Taylor Valley carbonates, we identify a reservoir inception time coincident with Marine Isotope Stage (MIS) 11. In contrast, for reservoir isolation to have begun during the next interglacial (MIS 9) would require an initial $\delta^{234}U$ in subglacial waters of >1000‰ (Fig. 3c), consistent with the lowest values observed in Elephant Moraine sample PRR50489. The formation of subglacial samples during subsequent interglacials (MIS 5, 7), along with documented ^{234}U accumulation during these times, is inconsistent with MIS 5 or 7 ice loss and rather point to an earlier reservoir isolation that permits ^{234}U accumulation to the values observed.

Discussion and Conclusions

Measured data from both EAIS precipitates and carbonates from the McMurdo Dry Valleys unequivocally record ^{234}U accumulation within fluids that initiated at $\delta^{234}U$ values lower than present (Fig. 3). Our documented accumulation does not reflect a ^{234}U system in steady state (black dashed, Fig. 3) and are thus inconsistent with fluids that have experienced isolation and contact with rocks on million-year durations. Collectively these observations are inconsistent with models for extreme EAIS stability on million-year timescales. Rather, these data require that the subglacial reservoir within the low elevation Wilkes Basin began at a lower $\delta^{234}U$ and remained at least partially isolated with respect to uranium for only ~400 ka. Without such isolation ^{234}U would not have accumulated and requires that over the last ~400 ka, the evacuation and replacement of ^{234}U enriched fluids from the ice sheet base was exceeded by ^{234}U enrichment. The accumulation of ^{234}U in this isolated to partially isolated reservoir implies ice stability over the last 400 ka. The lower $\delta^{234}U$ values inferred at MIS 10-11, however, imply that the replacement of ^{234}U enriched fluids, perhaps by flushing of basal waters or ice cap retreat, did outpace ^{234}U ingrowth at this time. This interpretation of the ^{234}U accumulation record in East Antarctica draws on the observed ^{234}U cycling in the Laurentide ice sheet, where ^{234}U-enriched subglacial waters were documented at the peak of Laurentide ice extent/volume (25 ka)[6], but the reservoir was released to global oceans in response to deglaciation[7]. Though any record of ^{234}U accumulation beneath the EAIS prior to MIS 11 is not reflected in the data presented here, we may infer from the documentation of ^{234}U enrichment beneath the Laurentide[6,7], Cordilleran[22], Iceland [31], Greenland [32] and Antarctic ice masses, that ^{234}U accumulation occurs in response to protracted rock-water contact in an isolated or partially isolated reservoir. Based on the documented response in Atlantic coral $\delta^{234}U_i$ to Laurentide deglaciation[7], we suggest that any pool of pre-MIS 11 ^{234}U-rich waters stored beneath the EAIS as well as Greenland and West Antarctica (discussed below), was released to the oceans, which may explain, in conjunction with diagenetic effects, why the $\delta^{234}U_i$ compositions of MIS 11 corals record a change in marine $\delta^{234}U_i$ compositions[33] a factor of 10 greater than the change recorded[7] in response to the most recent deglaciation .

There are few possible ice sheet responses to MIS 11 warming that may have led to the observed cycling in $\delta^{234}U$. Increased warming could have led to enhanced glacial ablation on the EAIS, complete with surface melting, moulin formation and flushing basal waters that reset the ^{234}U accumulation at the base of the ice. The basal flushing volumes required to lower the $\delta^{234}U$ within subglacial waters are 3-4 orders of magnitude higher than estimates of present subglacial water volumes (Extended data Fig. 5, methods and SI). The question then becomes: was MIS 11 warming sufficient to induce such surface melting and meltwater penetration to the bed, within the Wilkes basin? Ice sheet models[14] and our current climate do not support this response and instead show that EAIS retreat within the marine basins would have to be driven by ocean-ice interactions, which would occur prior to reaching sufficient warming to permit surface melting and basal flushing at such high volumes. In short, polar conditions like today would persist on the ice surface even as the ice mass retreats within the low elevation marine basins in response to warming oceans. Thus, an alternative explanation to basal flushing for the observed cycling in $\delta^{234}U$ is that the Wilkes Basin grounding line moved closer to the precipitate sampling locations during MIS 11 as a result of ice interaction with warming oceans (Fig. 1). Under such a mechanism for removal of ^{234}U enriched waters, the geographic position of subglacial precipitates could be used to infer whether ice in a specific location remained stable or was lost at a particular point in time. For example, the

Elephant Moraine samples derive from a glacial catchment that extends into the Wilkes basin ~700 km inboard from the current grounding line (Fig. 1), implying significant retreat within the Wilkes Basin at MIS 11. Such a collapse is plausible: the inland-sloping topography of Wilkes Basin makes grounding line retreat in this region susceptible to a positive feedback that could produce more than 800 km of grounding line migration[13]. And while basal flushing and grounding line retreat could work hand-in-hand to some extent, the width of an ablation zone within a retreating ice sheet at high latitudes would be sufficiently narrow (<30km)[34,35] to render the relative contribution of flushing to resetting ^{234}U accumulation relatively minor when compared to the hundreds of kilometers of grounding line migration required to affect the samples studied here. In other words, these samples are so far inland, and the conditions are still so cold, that grounding line retreat must be the dominant mechanism for ^{234}U resetting. If ice retreated from Wilkes Basin, which lies below sea level, it would fill with seawater, replacing or mixing with high $\delta^{234}U$ composition waters. Following MIS 11, the subsequent readvance of ice over marine sediments with connate seawater would impart marine signatures on subglacial waters, consistent with the geochemical, isotopic and biogeochemical evidences for marine sourcing of MDV fluids[10,12]. In addition, proposed ice loss at MIS 11 within the Wilkes basin is consistent with glaciological evidence and with maximum exposure ages at Elephant moraine of ~400 ka (see methods for further discussion). The accumulation of ^{234}U at Elephant moraine throughout MIS 5, 7 and very likely 9 (Fig. 1) suggests that any ice loss during these shorter duration warmer periods, as resolved by offshore sedimentary records[17], did not reach this far back into the Wilkes Basin. And indeed, offshore sedimentary archives record a more pronounced on-continent weathering signal during MIS 11 as compared to subsequent interglacials[17]. At the warmer and longer MIS 11 interglacial the EAIS grounding line must have retreated to the proximity of this sample location, ~700km inland from the current coastline. A minimum contribution of Wilkes Basin collapse to global sea level at MIS 11 can be estimated if we assume that : 1) grounding line retreat was not accompanied by ice sheet thickening, as invoked for warmer Pliocene conditions[36], and 2) ice volumes prior to MIS 11 warming were at least comparable with the current, well-known ice volumes[13]. Both assumptions are likely safe. Models predict[36] ice thickening during Pliocene warmth where low sea ice coverage leads to increased precipitation, conditions that do not apply to the colder Pleistocene. Similarly, ice volumes within the Wilkes Basin prior to MIS 11 warming are likely comparable or *greater* than present. Preceding MIS 11 warming, MIS 12 was one of the coldest glacial periods of the Pleistocene[2] while currently, during one of the warmest Pleistocene interglacials, the basin contains ice volumes that would contribute an estimated ~3-4 m[13] to global sea level rise in response to the reported extent of Wilkes Basin grounding line retreat.

The record presented here tightly brackets the EAIS response to a warming world: 1-2 °C warming during the long MIS 11 interglacial, the warmest temperatures observed since ~2 Ma, resulted in hundreds of kilometers of grounding line retreat, while similar temperatures during the subsequent and shorter MIS 5 and 9 interglacials did not result in a comparable retreat. Our interpretation of a diminished MIS 11 ice sheet in the Wilkes Basin that contributed meters to global sea level is also consistent with distal geologic data for sea level during this interglacial. Sea level reconstructions resulting from MIS 11 warming are up to 4 m higher than the subsequent interglacials suggesting the Wilkes Basin may account for the difference in sea level highstands. The 6-13 m[3] MIS 11 highstands has been attributed to reflect near complete collapse of the Greenland (4.5-6 m[37]) and West Antarctic (3.2-5 m[38]) ice sheets alone[3], which only can account for a maximum of 11 m. The 700 km of grounding line retreat reported here would very likely result in several meters of global sea level rise, suggesting that MIS 11 highstands greater than 11 m and perhaps as high as 13 m may occur in response to 1-2 °C of global warming.

References

1 Dutton, A. *et al.* Sea-level rise due to polar ice-sheet mass loss during past warm periods. *science* **349**, aaa4019 (2015).

2 Lisiecki, L. E. & Raymo, M. E. A Pliocene-Pleistocene stack of 57 globally distributed benthic δ18O records. *Paleoceanography* **20** (2005).

3 Raymo, M. E. & Mitrovica, J. X. Collapse of polar ice sheets during the stage 11 interglacial. *Nature* **483**, 453, doi:10.1038/nature10891 (2012).

4 Sugden, D. E., Marchant, D. R. & Denton, G. H. The case for a stable East Antarctic ice sheet: the background. *Geografiska Annaler: Series A, Physical Geography* **75**, 151-154 (1993).

5 Sugden, D. E. *et al.* Preservation of Miocene glacier ice in East Antarctica. *Nature* **376**, 412 (1995).

6 Refsnider, K. A. *et al.* Subglacial carbonates constrain basal conditions and oxygen isotopic composition of the Laurentide Ice Sheet over Arctic Canada. *Geology* **40**, 135-138 (2012).

7 Chen, T. *et al.* Ocean mixing and ice-sheet control of seawater 234U/238U during the last deglaciation. *Science* **354**, 626-629 (2016).

8 Henderson, G. M., Hall, B. L., Smith, A. & Robinson, L. F. Control on (234U/238U) in lake water: A study in the Dry Valleys of Antarctica. *Chemical Geology* **226**, 298-308 (2006).

9 Hendy, C. H., Healy, T. R., Rayner, E. M., Shaw, J. & Wilson, A. T. Late Pleistocene glacial chronology of the Taylor Valley, Antarctica, and the global climate. *Quaternary Research* **11**, 172-184 (1979).

10 Lyons, W. B. *et al.* The geochemistry of englacial brine from Taylor Glacier, Antarctica. *Journal of Geophysical Research: Biogeosciences* **124**, 633-648 (2019).

11 Mikucki, J. A. *et al.* Deep groundwater and potential subsurface habitats beneath an Antarctic dry valley. *Nature communications* **6**, 6831 (2015).

12 Mikucki, J. A. & Priscu, J. C. Bacterial diversity associated with Blood Falls, a subglacial outflow from the Taylor Glacier, Antarctica. *Appl. Environ. Microbiol.* **73**, 4029-4039 (2007).

13 Mengel, M. & Levermann, A. Ice plug prevents irreversible discharge from East Antarctica. *Nature Climate Change* **4**, 451 (2014).

14 DeConto, R. M. & Pollard, D. Contribution of Antarctica to past and future sea-level rise. *Nature* **531**, 591 (2016).

15 Gasson, E., DeConto, R. & Pollard, D. Antarctic bedrock topography uncertainty and ice sheet stability. *Geophysical Research Letters* **42**, 5372-5377 (2015).

16 Huybrechts, P. Glaciological modelling of the Late Cenozoic East Antarctic ice sheet: stability or dynamism? *Geografiska Annaler: Series A, Physical Geography* **75**, 221-238 (1993).

17 Wilson, D. J. *et al.* Ice loss from the East Antarctic Ice Sheet during late Pleistocene interglacials. *Nature* **561**, 383 (2018).

18 Kigoshi, K. Alpha-recoil thorium-234: dissolution into water and the uranium-234/uranium-238 disequilibrium in nature. *Science* **173**, 47-48 (1971).

19 Hallet, B. Deposits formed by subglacial precipitation of $CaCO_3$. *Geological Society of America Bulletin* **87**, 1003-1015 (1976).

20 Faure, G., Hoefs, J., Jones, L. M., Curtis, J. B. & Pride, D. E. Extreme 18O depletion in calcite and chert clasts from the Elephant Moraine on the East Antarctic ice sheet. *Nature* **332**, 352 (1988).

21 Hallet, B. Subglacial silica deposits. *Nature* **254**, 682 (1975).

22 Blackburn, T. *et al.* Composition and formation age of amorphous silica coating glacially polished surfaces. *Geology* **47**, 347-350 (2019).

23 Aharon, P. Oxygen, carbon and U-series isotopes of aragonites from Vestfold Hills, Antarctica: clues to geochemical processes in subglacial environments. *Geochimica et Cosmochimica Acta* **52**, 2321-2331 (1988).

24 Frisia, S. *et al.* The influence of Antarctic subglacial volcanism on the global iron cycle during the Last Glacial Maximum. *Nature communications* **8**, 15425 (2017).

25 Fitzpatrick, J. J., Muhs, D. R. & Jull, A. J. T. Saline minerals in the Lewis Cliff ice tongue, Buckley Island quadrangle, Antarctica. *Contributions to Antarctic Research I* **50**, 57-69 (1990).

26 Goodwin, I. D. *et al.* Modern to Glacial age subglacial meltwater drainage at Law Dome, coastal East Antarctica from topography, sediments and jökulhlaup observations. *Geological Society, London, Special Publications* **461**, 215-230 (2018).
27 Chutcharavan, P. M., Dutton, A. & Ellwood, M. J. Seawater 234U/238U recorded by modern and fossil corals. *Geochimica et Cosmochimica Acta* **224**, 1-17 (2018).
28 Berry Lyons, W., Frape, S. K. & Welch, K. A. History of McMurdo Dry Valley lakes, Antarctica, from stable chlorine isotope data. *Geology* **27**, 527-530 (1999).
29 Poreda, R. J., Hunt, A. G., Lyons, W. B. & Welch, K. A. The helium isotopic chemistry of Lake Bonney, Taylor Valley, Antarctica: Timing of late Holocene climate change in Antarctica. *Aquatic Geochemistry* **10**, 353-371 (2004).
30 Warrier, R. B., Castro, M. C., Hall, C. M., Kenig, F. & Doran, P. T. Reconstructing the evolution of Lake Bonney, Antarctica using dissolved noble gases. *Applied Geochemistry* **58**, 46-61 (2015).
31 von Strandmann, P. A. E. P. *et al.* Riverine behaviour of uranium and lithium isotopes in an actively glaciated basaltic terrain. *Earth and Planetary Science Letters* **251**, 134-147 (2006).
32 Arendt, C. A. *et al.* Influence of glacial meltwater on global seawater δ 234 U. *Geochimica et Cosmochimica Acta* **225**, 102-115 (2018).
33 Bard, E., Fairbanks, R. G., Hamelin, B., Zindler, A. & Hoang, C. T. Uranium-234 anomalies in corals older than 150,000 years. *Geochimica et Cosmochimica Acta* **55**, 2385-2390 (1991).
34 Catania, G. A., Neumann, T. A. & Price, S. F. Characterizing englacial drainage in the ablation zone of the Greenland ice sheet. *Journal of Glaciology* **54**, 567-578 (2008).
35 Bøggild, C. E., Brandt, R. E., Brown, K. J. & Warren, S. G. The ablation zone in northeast Greenland: ice types, albedos and impurities. *Journal of Glaciology* **56**, 101-113 (2010).
36 Yamane, M. *et al.* Exposure age and ice-sheet model constraints on Pliocene East Antarctic ice sheet dynamics. *Nature Communications* **6**, 1-8 (2015).
37 Reyes, A. V. *et al.* South Greenland ice-sheet collapse during marine isotope stage 11. *Nature* **510**, 525 (2014).
38 Gomez, N., Mitrovica, J. X., Tamisiea, M. E. & Clark, P. U. A new projection of sea level change in response to collapse of marine sectors of the Antarctic Ice Sheet. *Geophysical Journal International* **180**, 623-634 (2010).
39 Fretwell, P. *et al.* Bedmap2: improved ice bed, surface and thickness datasets for Antarctica. (2013).
40 Greene, C. A., Gwyther, D. E. & Blankenship, D. D. Antarctic Mapping Tools for Matlab. . *Computers & Geosciences* **104** 151-157 (2017).
41 Pattyn, F. Antarctic subglacial conditions inferred from a hybrid ice sheet/ice stream model. *Earth and Planetary Science Letters* **295**, 451-461 (2010).

Figure 1. Base map of East Antarctica showing bedrock topography from Bedmap2[39,40] (grey-scale contour) overlain by the contour line at sea level (0 m). White dots are known subglacial lakes[41]. Dashed red lines shows model predicted grounding line in response to 1.8 ºC of ocean warming and corresponds to ice volumes equivalent to 3-4m of sea level rise[13]. Subglacial precipitate locations: PM: Pensacola mountains, LC: Lewis Cliff[25], EM: Elephant Moraine, BV: Boggs Valley[24], AB: Aurora Basin[26], MDV: McMurdo Dry Valley[8-10](contemporary waters and lake carbonates) SW: Seawater[8]. Data point size indicates age, while color indicates initial $\delta^{234}U$ composition.

Figure 2. Model ^{234}U ingrowth histories in waters from injection by alpha-recoil incurred by the decay of ^{238}U housed within sediments. The ^{234}U system reaches within 1% of steady state before ~1500 ka, after which time the $\delta^{234}U_i$ recorded by precipitates would remain constant over time. If changes in $\delta^{234}U_i$ over time are observed this requires: 1) lower $\delta^{234}U$ starting fluids and 2) isolation to permit ^{234}U accumulation. Differences in sediment characteristics (e.g. porosity, U content) can vary across a continent, thus producing a range in steady state $\delta^{234}U$ ($\delta^{234}U_{SS}$).

Figure 3. Measured and modeled ^{234}U ingrowth histories for the Wilkes basin **a**. Formation age vs. the initial $\delta^{234}U$ for EAIS subglacial precipitates, MDV waters and lake carbonates. Numbered time scale corresponds to Marine Isotope Stages. See Figure 1 for locations. All measurement uncertainties are ±2σ s.d. Blue and red curves correspond to maximum likelihood modeled ingrowth curves for sample Elephant Moraine sample PRR50489 where the color indicates the initial $\delta^{234}U$ of a subglacial reservoir: 500 ‰ (red) and 100 ‰ (blue) which correspond to the lowest compositions observed in Taylor Valley and Elephant Moraine (PRR39222), respectively.

Purple lines show calculated $\delta^{234}U_i$ for PRR39222 over 0-450 ka with superimposed $\delta^{234}U$ ingrowth histories (black arrows) from assumed calcite precipitation rates (see Extended Data Fig. 3 for further discussion). Grey curves show the model projections for scenarios with a 400 ka onset and variations in sediment characteristics from figure 2. Dashed line in **a** show the predictions for a ^{234}U system after ~1 My of rock-water contact. The example maximum likelihood estimate in (**b**) assumes an initial $\delta^{234}U$ for the reservoir of 145‰ and identifies a best fit path with an inception time of 435 +20/-25 ka (95% confidence interval, black uncertainty ellipse) **c**. Uncertainty in reservoir inception time is dominated by the initial $\delta^{234}U$ of the hydrologic reservoir. Gray polygon outlines 95% confidence envelope of best-fit conditions. Independent of initial $\delta^{234}U$ of reservoir, best fit curves identify near identical ingrowth histories and $\delta^{234}U_{SS}$ (overlapping blue and red curves shown in **a**).

Methods:

U-series methods: ^{234}U-^{230}Th dates were produced at the UCSC Keck Isotope Laboratory. Samples digestions were carried out using either 7N HNO_3 (calcite) or concentrated HF + HNO_3 (opal). Samples were spiked with a gravimetrically calibrated mixed ^{229}Th-^{236}U tracer and dried down. U and Th separates were purified using an ion chromatography procedure that used 1ml of AG1-X8 anion resin. Total procedural blanks for U and Th were < 5 pg and minor relative to sample sizes. Uranium isotopic measurements were conducted using the IsotopX X62 Thermal Ionization Mass Spectrometer housed at UCSC and measured uranium as UO_2 using a Si-gel emitter. Uranium compositions were corrected for oxide isobaric interferences following [42]. Mass dependent fractionation correction was applied using a linear correction with correction factor determined from long-term measurement of standards. Uranium dead times for the Daly were calibrated using NBS U-500. Accuracy of the uranium method was evaluated using Uranium standard NBS4321. Extended data figure 4 shows NBS4321 analyses measured over the duration of this study. Thorium isotopic determinations used the UCSC TIMS, by graphite loading and a Daly peak hopping routine. Thorium fractionation and deadtime were estimated by running NBS U 500 as a metal. ^{234}U-^{230}Th date accuracy were tested using MIS 5e coral dated by Hamelin and others[43], an in house opal standard in secular equilibrium and subglacial carbonate precipitate previously dated by Frisia and others[24] (Table 3). U-Th ages are calculated using codes designed at UCSC. Decay constants for all data and models were from Cheng and others[44]. All uncertainties are reported at 2σ. Mass spectrometry methods are described in greater detail in the supplementary information.

Simulating porewater $\delta^{234}U$ evolution: The $\delta^{234}U$ enrichment in subglacial settings could result from direct injection or preferential leaching of ^{234}U from glacial sediments into subglacial waters. Preferential leaching of ^{234}U relative to ^{238}U has experimentally been shown to increase fluid $\delta^{234}U$ to marine-like compositions on laboratory timescales, however there is a finite pool of leachable ^{234}U in rocks, such that on longer residence times (>10^4 yrs) both natural and experimental waters reveal sub-marine $\delta^{234}U$ [45]. In the EAIS rather, the accumulation to high $\delta^{234}U$ values (4000 ‰) and the topology of $\delta^{234}U_i$ with time, both match the model predictions of ^{234}U accumulation by direct injection into fluids incurred during the decay of ^{238}U housed within subglacial sediments. Collectively, these data point to a subglacial water reservoir that initiated with low $\delta^{234}U$ compositions that then increased by ^{234}U recoil-injection but has yet to reach a steady state $\delta^{234}U$ composition, for which the ^{234}U-system, would be attained after approximately 1 million years of rock-water contact. The time-dependent evolution of ^{234}U in sediment porewaters may be described by a model presented in the supplementary information. Using this model, simulated $^{234}U/^{238}U$ fluid evolutions are evaluated by comparison with the measured data using a maximum likelihood test (also detailed in the supplementary information).

The influence of hydrological flushing on $\delta^{234}U$ of subglacial waters: Our analyses of subglacial precipitates record a progressive increase in $\delta^{234}U$ of subglacial waters, from which these precipitates formed, since MIS 11, when the $\delta^{234}U$ reservoir has been reset to very low values. We consider here (and within the supplementary information where the model is described in full with equations) whether this MIS 11 re-setting event may have had to do simply with an increase in basal melting, e.g., due to thickening of the ice sheet caused by a warming-induced increase in precipitation[46], and the associated increase in hydrological flushing rates of the subglacial water reservoir. The results of this model show that only very short flushing timescales, <10 years, result in low values of the steady-state activity ratio. We expect that comparably low values have been reached during the event which reset the $\delta^{234}U$ values during MIS 11 (Figure 3). This result applies to other combinations of parameters beyond the ones illustrated in Extended Data Figure 5. For instance, similar curves can be obtained for a weathering timescale of 10 million years as long as the ^{234}U ejection factor is about ten times larger than the values shown in the above figure, which would require finer-grained subglacial sediments. It is useful at this point to estimate, for reference, what is the flushing rate for the subglacial zone of the modern Antarctic ice sheet. Pattyn[41] used a numerical ice sheet model to calculate that basal melting produces approximately 65 km^3 of melt per year. Assuming no significant change in subglacial water storage and allowing for some losses to infiltration into deep groundwater systems (e.g., [47]) and to basal freezing, this means that the continental-scale hydrological throughflow rate is approximately a few 10s of km^3 per year. Dowdeswell and Siegert [48] estimated that subglacial Antarctic lakes alone contain about 10,000 km^3. Another large water reservoir that is hydrologically connected to the basal meltwater system is the porewater in subglacial tills that exchanges chemical species through Darcian flow, physical deformation accompanying ice sheet motion, and ionic diffusion (e.g., [49]). It would take less than 2m-thick till layer on average across the entire base of the ice sheet for the porewater reservoir to amount to an additional 10,000 km^3 of subglacial storage, assuming reasonable porosity of 35%. Hence, the total subglacial water storage is similar to a few tens of thousands of km^3. Dividing this volume by the throughflow rate of a few tens of km^3 per year yields an approximate flushing timescale for the modern Antarctic ice sheet of ~1,000 years. According to Extended data Figure 5, such timescale would allow buildup of steady-state U^{234} activity ratios comparable to the ones observed in our samples (1000s of ‰). However, the flushing timescale would have to be lowered by about 2-3 orders of magnitude, to 1-10 years, to bring the steady-state $\delta^{234}U$ to values as low as a few hundred ‰. Although, for simplicity, we have focused here on the discussion of the steady-state $\delta^{234}U$, we have also performed calculations of the time evolution of $\delta^{234}U$ for a large range of the control parameters f, τ_f, and, τ_w. We find that the flushing timescale is the predominant timescale which controls the rate of $\delta^{234}U$ convergence towards its steady-state value. This is particularly the case when the flushing timescale is much shorter than the mean lifetime of ^{234}U ($\tau_f << \tau_4$ = 354,260 years) because the time-dependent, exponential, terms in Equations 8 and 10 are either dependent on $1/\tau_f$ or on the sum $(1/\tau_f + 1/\tau_4)$. When the flushing timescale is short, the $1/\tau_4$ term becomes negligibly small and the evolution of $\delta^{234}U$ with time depends only on exponential terms governed by t/τ_f. This means that a decrease in the flushing timescale to small values, e.g., 1-10 years, from a larger value (e.g., between 100 and 10,000 years) would very quickly bring the subglacial $\delta^{234}U$ close to its new and lower steady-state value. For instance, $\delta^{234}U$ would be within 5% of the steady-state value after only 3-30 years have elapsed following the decrease of the flushing timescale to 1-10 years.

There is no reason to suspect that the total volume of water stored beneath the ice sheet was lower by 2-3 orders of magnitude during MIS11 than today. In fact, this volume is unlikely to change much through time and temporal variations in the flushing timescale must be largely controlled by variations in the water throughflow rate, which would have to increase by 2-3 orders of magnitude compared to today to significantly lower subglacial $\delta^{234}U$. Hence, the ice sheet base would have to be flushed at the rate of ~1,000 to ~10,000 km^3 per year as compared to the modern rate of ~10 km^3 per year. This kind of increase cannot be attributed to an increase in basal melting rate, say due to ice sheet thickening during MIS 11, which at most could increase the throughflow rate by a small factor, e.g., a factor of two. The only process that can introduce enough water to the ice sheet base to lower the flushing timescale by a few orders of magnitude is the penetration of surface meltwater to the ice base through moulins and fractures, as it happens on Greenland ice sheet and temperate mountain glaciers (e.g., [50,51]). Indeed, two prior studies of $\delta^{234}U$ in subglacial waters from beneath Athabasca Glacier and Greenland ice sheet do show very low values, 3-40 ‰ for the former[52] and 5-270‰ for the latter [32]. Athabasca Glacier subglacial zone is flushed on seasonal timescales[52] while Greenland basins examined in [32] can easily have 0.1-10 years timescales compatible with the range of values $\delta^{234}U$ observed there (Extended data Figure 5). In Greenland, however, these observed low $\delta^{234}U$ come from locations were mean annual temperatures in the ablation zone are warmer than -10ºC whereas most of the East Antarctic ice sheet surface is an accumulation zone with mean annual temperatures falling between -30ºC and -50ºC (e.g., [53]). Occurrence of sufficient surface melting that would lead to large enough meltwater penetration to the ice base over current Antarctic accumulation areas would require warming of a few dozens of degrees. Yet, the numerical ice sheet model[54] predict retreat of the ice sheet from subglacial basins such as Wilkes and Aurora with a much smaller thermal forcing accompanying the RCP8.5 scenario. This indicates that these marine-based regions of the ice sheet will experience grounding line retreat due to ice-ocean interactions before an ablation zone with high surface melt and significant water penetration to the bed develops over these regions. Therefore, our favored interpretation for the low value of $\delta^{234}U$ around the time of MIS 11 is ice sheet retreat followed by seawater intrusion into subglacial basins located below sea level rather than a dramatic decrease in the flushing timescale that is not accompanied by an ice sheet retreat.

Sample descriptions and field settings: New data presented here are from samples collected from the Pensacola Mountains, and Elephant Moraine both within East Antarctica. A total of 3 samples were dated at multiple horizons (PRR16794, PRR50489, PRR39222). These samples were provided by the Byrd Polar Rock Repository at The Ohio State University[55]. Sample PRR16794 at the Pensacola Mountains is entirely calcite, exhibits a fine scale internal layering related to precipitate growth (Extended Data Fig. 1). The uranium content is 5 ppm. U-Th dates between the top and bottom are within uncertainty at ~200 ka but $\delta^{234}U_i$ values are resolvable from top to bottom and range from 1875-1990‰ (Table S1). The $\delta^{18}O_{smow}$ of calcite is -9.3‰ (Table 2). Sample PRR50489 at Elephant Moraine consists of inter-bedded calcite and opal, exhibited in discrete layering related to precipitate growth (Extended Data Fig. 2). The $\delta^{18}O_{smow}$ of the calcite in this sample is -19.87‰ (Table 2). The uranium content of calcites are <1ppm. Opal U concentrations span from 10-30 ppm. U-Th dates for opals between the top and bottom span >100 thousand years in duration and exhibit $\delta^{234}U_i$ values of 1470-2000‰ (Table 1). Sample PRR39222 at Elephant Moraine is a precipitate of black calcite. Sample PRR39222 consists of calcite sparite crystals that radiate upwards and out from nucleation surfaces. Organic material is abundant. Silicates are also present but less common. The $\delta^{18}O_{smow}$ of calcite from this sample is -19.45 ‰ (Table 2). Sample bulk sample Uranium concentrations are <1 ppm and $\delta^{234}U$ measured values range from 40-140‰ and scale with stratigraphic position in the sample (Extended Data Fig. 3, Table 1). The U and Th composition of a calcite digested in 7N HNO_3 will represent a mixture of uranium and thorium sourced from: 1) the calcite; 2) organics (which are abundant); 3) U and Th adsorbed onto silicates. Because of adsorbed thorium, we cannot determine a U-Th date and we've restricted our interpretation of PRR39222 to the uranium composition alone. However, the uranium isotopic composition is also a mixture of the 3 above sources but it can be demonstrated that the uranium sourced from the organics or adsorbed onto the surface of detrital silicates is in isotopic equilibrium with the waters that produce the calcite. A definitive test as to whether PRR39222 reliably records subglacial fluid compositions is provided by calcite analysis from sample PRR50489. Unlike PRR39222, PRR50489 has opals that reliably record the ^{234}U ingrowth within subglacial waters. The calcite measurement from PRR50489 yields values concordant with the values for opal that lie both stratigraphically above and below (Table 1). This strongly supports the argument that the bulk calcite digestion, despite having multiple sources of uranium, reliably records the uranium composition of the waters. The calcite from PRR50489 is very similar to PRR39222 and thus can serve as a proxy. Similarities include: 1) High Th/U; 2) crystal morphology, of radiating sparite crystals and black color; and 3) nearly identical $\delta^{18}O$ and $\delta^{13}C$ (Table 2).

Elephant moraine is a supraglacial moraine—an intra-ice site of sediment and rock accumulation of a once deeply residing section of dirty basal ice. The exhumation of this basal ice section occurs as East Antarctic ice flows off the high polar plateau (>2000m), and into the western slopes of the Transantarctic Mountains at an elevation of 120m below the plateau[56]. As flowing ice interacts with the underlying bedrock topography this basal layer is transported upwards towards the ice surface[56]. Surrounding the moraine is a blue-ice area, where there is significant loss of snow and ice to sublimation. This blue ice is just a small section of a larger sublimation belt that occurs as the thick ice of the EAIS flows eastward and is blocked by the Transantarctic Mountains[56]. The only exception to EAIS termination within such a sublimation zone is where outlet glaciers are squeezed through the major valleys cutting across the Transantarctic Mountains, such as Taylor glacier, which occupies Taylor Valley (See below for further discussion).. The occurrence of upturned ice sections from the base of the EAIS along the western flank of the Transantarctic mountains is not uncommon. Several such sections [25,55-58], marked by both blue-ice sections bearing meteorites[58] as well as exhumed dirty basal ice layers which can contain subglacial precipitates such as those found at Elephant Moraine, Lewis Cliff [25] and in proximity to the Pensacola Mountains[55] (Fig. 1). The subglacial precipitates that form at the base of the EAIS become frozen into this debris-laden ice layer and are exhumed along with sediments and clasts. Ice ablation at the surface leaves the precipitate samples "stranded." The precipitates are relatively rare compared to other lithologies. It has been suggested by Taylor[59] and reviewed by Faure and Mensing[56] that the timing of supraglacial moraine inception is directly linked with the timing of thinning of the East Antarctic ice sheet. These authors hypothesized that if East Antarctica were thicker the ice flowing over the bedrock protrusion beneath Elephant moraine would have a more muted surface expression than that of a supraglacial moraine. Under this thick ice condition, the underlying topography would induce an inflection in the ice surface but would be limited to producing a "ramp" that may have crevasses and ice pinnacles at its crest. Under such thick-ice conditions, the EAIS dirty basal ice would not reach the surface. If the ice were to thin in response to climate, the exhumed basal ice would intersect the surface, initiating the formation of the supraglacial moraine. As such, an estimate on the timing of ice thinning can be constrained by estimates on the duration for which morainal materials have resided there, which is provided by exposure dating. Cosmogenic exposure ages exist for meteorites found within proximity (<1km) of the moraine in blue ice areas. The longest exposed meteorite dates to 370 ka[60] suggesting that Elephant Moraine and the thinning of EAIS ice initiated no sooner than the very end of MIS 11 boundary.

The McMurdo Dry Valleys are the largest rock oasis of Antarctica, where land terminating glaciers permit subglacial brines to emanate onto the surface or into proglacial lakes[11]. One of the Dry Valleys, Taylor Valley is occupied by Taylor Glacier, an outlet glacier of the East Antarctic ice sheet, and is one of the many narrow mountain passes through which the East Antarctic ice sheet extrudes as it flows from the high polar plateau towards the coast. Subglacial discharge reaches the surface at the snout of Taylor Glacier. There hypersaline fluids emanate seasonally in what is referred to as “Blood Falls” due to the occurrence of iron oxides that form upon oxidation of soluble iron[10,12,61]. Subglacial discharge of brines is also detected, geochemically at depth within the proglacial lake (lake Bonney) that abuts Taylor Glacier[8,62]. Surveys using airborne transient electromagnetics to image resistivity identify high-solute liquids connecting Lake Bonney to a subglacial region that extends up glacier for kilometers where increased ice thickness prevents further detection[11]. It’s been speculated that these fluids extend the length of Taylor Glacier back to the East Antarctic ice sheet[11]. The δ^{234}U composition of subglacial discharge in Taylor Valley ranges between 3500-5000 ‰ (Fig. 1, 3)[8,10]. Similarly ^{234}U enriched waters are observed in groundwater fed lakes in Wright Valley immediately to the north of Taylor Valley[8] suggesting that such subglacial discharge plays a role in the formation and composition of these lakes as well. Such an observation suggests a shared source for Wright Valley and Taylor Valley fluids and supports speculation that all MDV fluids are sourced from beneath the EAIS. This fuels further speculation that such fluids occur throughout the EAIS but are more readily observed in locations where glaciers terminate on land. Within the MDV lakes, Holocene age carbonates record δ^{234}U compositions similar to modern waters[9]. Similar lakes are theorized to occupy Taylor Valley at each interglacial period over the last ~350 ka[9]. As discussed in the main text, the δ^{234}U composition of these past carbonates reflects sourcing from a ^{234}U enriched subglacial reservoir and that this reservoir increases in ^{234}U with time, suggesting a coevolution with fluids within the Wilkes Basin. In addition to the age constraints provided by the apparent ^{234}U ingrowth record (Fig. 3), noble gas measurements from the deep waters of the modern Lake Bonney fed by subglacial discharge[11] provide additional age constraints. Excess in both ^{4}He and ^{40}Ar up to 200x atmospheric values point to fluid isolation from the atmosphere and contact with rock on durations that exceed 200 ka[29,30]. This is a minimum estimate, as any dilution by surface waters, which do exist in the shallow waters of Lake Bonney, would yield an apparently younger date. While these workers suggest that such isolation occurred *in situ* within lake Bonney, a compelling documentation for glacial advance and retreat on glacial-interglacial timescales[9,63,64] which place Taylor Glacier, at times, occupying the extent of Taylor Valley and reaching the Ross Sea, imply that Lake Bonney is an ephemeral feature. In short, these waters did not reside in Lake Bonney for 200 ka because Lake Bonney did not exist then and was filled by ice during the documented expansions of Taylor Glacier. The detection of subglacial discharge beneath Taylor Glacier provides a solution[11]—the long term isolation of fluids occurred not in Lake Bonney but beneath the East Antarctic ice sheet prior to their passage beneath Taylor Glacier and into the proglacial Lake Bonney.

Data availability: All data used are included within the extended data and uploaded to Earthchem.org DOI: 10.26022/IEDA/111548

Code availability: Any codes used are available upon request

Method references.

42 Condon, D. J., McLean, N., Noble, S. R. & Bowring, S. A. Isotopic composition (238U/235U) of some commonly used uranium reference materials. *Geochimica et Cosmochimica Acta* **74**, 7127-7143.

43 Hamelin, B., Bard, E., Zindler, A. & Fairbanks, R. G. 234U/238U mass spectrometry of corals: How accurate is the UTh age of the last interglacial period? *Earth and Planetary Science Letters* **106**, 169-180 (1991).

44 Cheng, H., Edwards, R.L., Shen, C.-C., Polyak, V.J., Asmerom, Y., Woodhead, J., Hellstrom, J., Wang, Y., Kong, X., Spötl, C., 2013. Improvements in 230Th dating, 230Th and 234U half-life values, and U–Th isotopic measurements by multi-collector inductively coupled plasma mass spectrometry. *Earth and Planetary Science Letters* 371, 82-91.

45 Andersen, M. B., Erel, Y. & Bourdon, B. Experimental evidence for 234U–238U fractionation during granite weathering with implications for 234U/238U in natural waters. *Geochimica et Cosmochimica Acta* **73**, 4124-4141 (2009).

46 Prentice, M. L. & Matthews, R. K. Tertiary ice sheet dynamics: The snow gun hypothesis. *Journal of Geophysical Research: Solid Earth* **96**, 6811-6827 (1991).

47 Christoffersen, P., Bougamont, M., Carter, S. P., Fricker, H. A. & Tulaczyk, S. Significant groundwater contribution to Antarctic ice streams hydrologic budget. *Geophysical Research Letters* **41**, 2003-2010 (2014).

48 Dowdeswell, J. A. & Siegert, M. J. Ice-sheet numerical modeling and marine geophysical measurements of glacier-derived sedimentation on the Eurasian Arctic continental margins. *Geological Society of America Bulletin* **111**, 1080-1097 (1999).

49 Tulaczyk, S., Kamb, B. & Engelhardt, H. F. Estimates of effective stress beneath a modern West Antarctic ice stream from till preconsolidation and void ratio. *Boreas* **30**, 101-114 (2001).

50 Howat, I. M., Joughin, I., Tulaczyk, S. & Gogineni, S. Rapid retreat and acceleration of Helheim Glacier, east Greenland. *Geophysical Research Letters* **32** (2005).

51 Howat, I. M., Tulaczyk, S., Waddington, E. & Björnsson, H. Dynamic controls on glacier basal motion inferred from surface ice motion. *Journal of Geophysical Research: Earth Surface* **113** (2008).

52 Arendt, C. A., Aciego, S. M., Sims, K. W. W. & Aarons, S. M. Seasonal progression of uranium series isotopes in subglacial meltwater: Implications for subglacial storage time. *Chemical Geology* **467**, 42-52 (2017).

53 Bréant, C., Martinerie, P., Orsi, A., Arnaud, L. & Landais, A. Modelling firn thickness evolution during the last deglaciation: constraints on sensitivity to temperature and impurities. *Climate of the Past* **13**, 833-853 (2017).

54 Golledge, N. R. *et al.* The multi-millennial Antarctic commitment to future sea-level rise. *Nature* **526**, 421 (2015).

55 The Polar Rock Repository (PRR), B. P. a. C. R. C. B., Ohio State University: Geological samples available for research from the PRR. NOAA National Centers for Environmental Information. doi:10.7289/V5RF5S18 2019.

56 Faure, G. & Mensing, T. M. *The Transantarctic Mountains: Rocks, ice, meteorites and water*. (Springer Science & Business Media, 2010).

57 Faure, G. & Taylor, K. S. The geology and origin of the Elephant Moraine on the east antarctic ice sheet. *Antarctic Journal of the United States* **20**, 11 (1985).

58 Cassidy, W., Harvey, R., Schutt, J., Delisle, G. & Yanai, K. The meteorite collection sites of Antarctica. *Meteoritics* **27**, 490-525 (1992).

59 Taylor, K. S. Lithologies and distribution of clasts in the elephant moraine, Allan Hills South Victoria Land, Antarctica. (1986).

60 Nishiizumi, K., Elmore, D. & Kubik, P. W. Update on terrestrial ages of Antarctic meteorites. *Earth and Planetary Science Letters* **93**, 299-313 (1989).

61 Lyons, W. B. *et al.* Halogen geochemistry of the McMurdo Dry Valleys lakes, Antarctica: clues to the origin of solutes and lake evolution. *Geochimica et Cosmochimica Acta* **69**, 305-323 (2005).

62 Lyons, W. B. *et al.* Strontium isotopic signatures of the streams and lakes of Taylor Valley, Southern Victoria Land, Antarctica: chemical weathering in a polar climate. *Aquatic Geochemistry* **8**, 75-95 (2002).

63 Brook, E. J. *et al.* Chronology of Taylor Glacier advances in Arena Valley, Antarctica, using in situ cosmogenic 3He and 10Be. *Quaternary Research* **39**, 11-23 (1993).

64 Bockheim, J. G., Prentice, M. L. & McLeod, M. Distribution of glacial deposits, soils, and permafrost in Taylor Valley, Antarctica. *Arctic, Antarctic, and Alpine Research* **40**, 279-286 (2008).

Acknowledgments: Thanks to John Schutt, Gunter Faure and D Schmidt for their sample collection at Elephant Moraine and to Anne Grunow and the Byrd Polar Rock Repository for providing samples with a "PRR" prefix. Thanks to James Paces, Sidney Hemming and Troy Rasbury for their input. This research was funded by NSF 1644171 to TB and ST.

Author contributions: Blackburn wrote manuscript, lead this study, developed U-series methods. Edwards: model simulations, tracer calibration, U-series data reduction. Tulaczyk: data interpretation, modeling. Scudder: sample preparation, clean lab work. Piccione: clean lab work, tracer calibration. N. McLean: maximum likelihood model construction. Hallet: data interpretation. Zachos: oxygen isotopic analyses. Cheney, SEM imaging. Babbe: sample preparation, clean lab work.

Competing interest statement: Authors declare no competing interests.

Additional Information: Supplementary Information is available for this paper. Correspondence and requests for materials should be addressed to T. Blackburn. "Reprints and permissions information is available at www.nature.com/reprints".

Extended data captions

Extended Data Figure 1. Images of sample PRR16794. Sample shown in (a) plain light (with location of dated horizons) and (b) SEM/EDS compositional map showing variations in Mn.

Extended Data Figure 2. Images of sample PRR50489. Sample shown in (a) plain light (with location of dated horizons) and (b) SEM/EDS compositional map showing Ca and Si. Sample exhibits an angular unconformity, indicating that the sample physically moved beneath the ice before accumulation begins again.

Extended Data Figure 3. Model constraints on ^{234}U ingrowth history of PRR39222. Inset photo: Sample PRR39222 shown in plain light with location of $\delta^{234}U$ measurements. Main plot: The measured the $\delta^{234}U$ for PRR39222 at three horizons, resolves an increasing $\delta^{234}U$ from top to bottom (Table 1). Because of the high thorium contents, we cannot define a formation age and thus cannot identify a reliable initial $\delta^{234}U$. The purple curves in figure 3 represent the possible $\delta^{234}U_i$ values for the top (higher $\delta^{234}U$) and bottom for any formation time. What we do not know is the absolute time this sample formed or the duration it formed over. However, we do know that: 1) the $\delta^{234}U_i$ for the sample top and bottom must lie on these purple lines; 2) the sample must be younger than ~1.5My given that the measured $\delta^{234}U$ is not in secular equilibrium. In addition to these known conditions, we can assume that the calcite in PRR39222 likely formed very rapidly as indicated by: 1) morphology, specifically radiating clusters of blade-like sparite; 2) lack of unconformities; 3) shared $\delta^{18}O$ and $\delta^{13}C$ composition with rapidly forming calcite from PRR50489 which is constrained by geochronology. Data from the literature as well as the geochronologic constrains presented in table 1 provide limits on the rate of sub-ice calcite formation (0.5 mm/ka=shallow, 2 mm/ka middle, 5 mm/ka steep). Given a known sample dimension of 4.5 cm, any assumed precipitation rate translates to a time duration for sample formation of 10-90 ka. Assuming these durations, along with the requirement that the sample bottom and top intersects the purple curves shown in figure 3, permits definition of possible $\delta^{234}U_i$ ingrowth histories (black arrows, Fig. 3). The rate of modeled ^{234}U accumulation as recorded by PRR39222 is strongly controlled by assumed formation age with only a narrow time range yielding ^{234}U ingrowth histories consistent with the other Wilkes Basin fluid histories. For example, if the sample were to be have formed at 1000 ka (3), we predict a change in $\delta^{234}U_i$ of ~300% from the top to the bottom of this sample. Such rapid ingrowth histories result in $\delta^{234}U$ compositions that would result in $\delta^{234}U$ compositions that far exceeds anything observed in Antarctica (>6000 ‰). If however, the sample were to have formed at ~400 ka, the projected ingrowth histories would match both model projections and measured data for the Wilkes Basin. Only scenarios that place PRR39222 formation at roughly <500 ka yield projected ingrowth histories consistent with the blue curve. In addition to the above analysis, the occurrence of low $\delta^{234}U$ (<500 ‰) in subglacial fluids is apparently rare, having been identified in this region only in samples older than ~300 ka. Collectively this suggests that the ^{234}U ingrowth history recorded by PRR39222 is at least consistent with formation at ~400 ka.

Extended Data Figure 4. Long-term results of measurements of NBS 4321 (5.2919e-5 ± 0.013e-5 (0.25%)) at UCSC using an IsotopX X62, TIMS. All uncertainties are absolute 2σ SD.

Extended Data Figure 5. Steady state activity ratio of ^{234}U and ^{238}U as a function of the flushing timescale for three different values of the ^{234}U ejection factor. The dotted line shows the assumed level of $\delta^{234}U$ in meltwater. The assumed weathering timescale is 100 million years.

Table 1. U-Series data from EAIS precipitates. All uncertainties are absolute 2σ SD. Age uncertainties do not include decay constant uncertainties.

Table 2. Oxygen and carbon isotopic data from EAIS precipitates measured at the University of California, Santa Cruz Stable Isotope Laboratory on the Kiel IV and Thermo Mat253.

Table 3. U-series standard data collected at UCSC and at bottom, accepted ages. All uncertainties are absolute 2σ SD**.** Age uncertainties do not include decay constant uncertainties.

Table 4. Legacy U-series recalculated using refined decay constants 2σ SD**.** Age uncertainties do not include decay constant uncertainties.

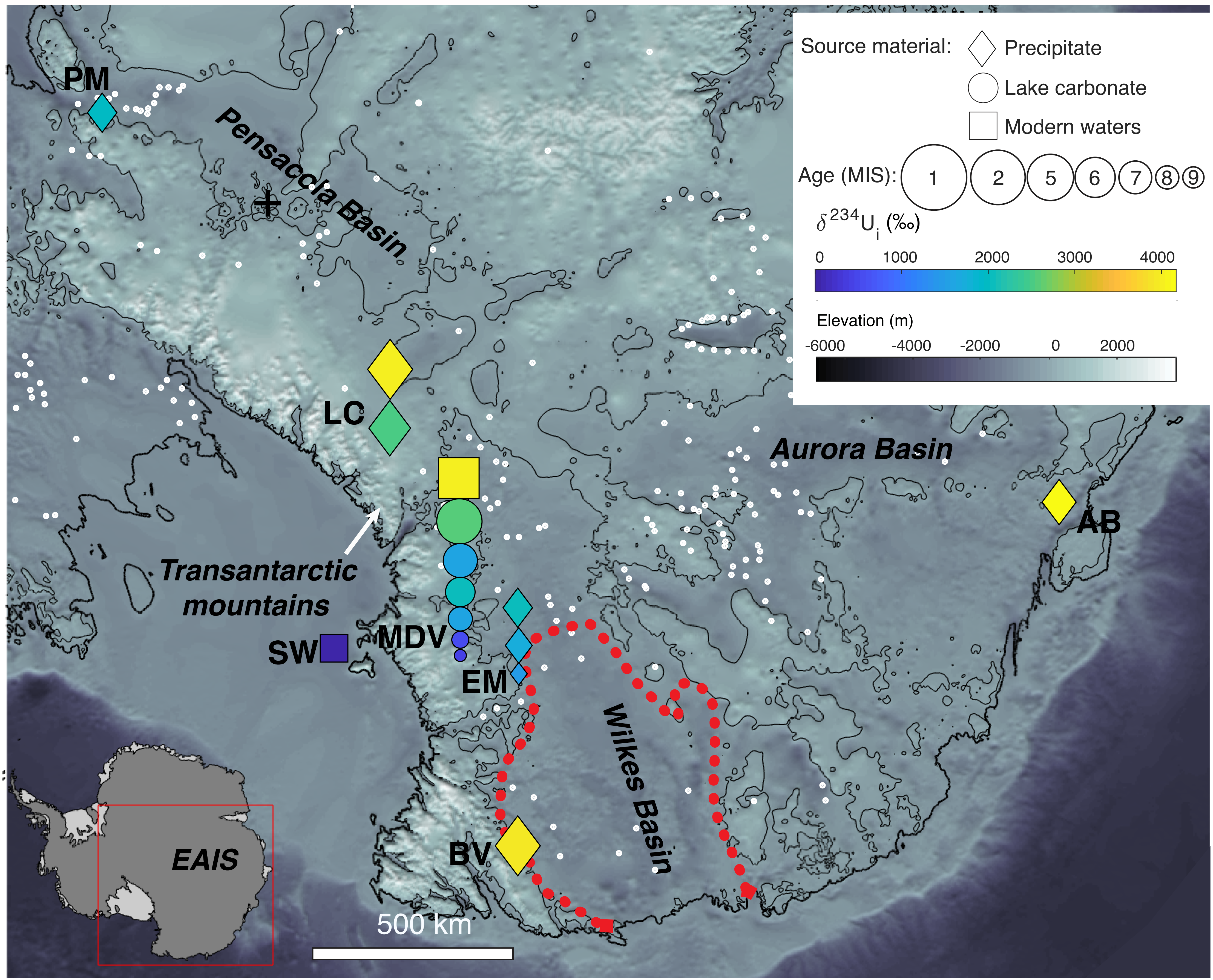

Source material:
Precipitate
Lake carbonate
Modern waters
Age (MIS):
1
2
5
6
7
8
9
$\delta^{234}U_i$ (‰)
0
1000
2000
3000
4000
Elevation (m)
-6000
-4000
-2000
0
2000
PM
Pensaccla Basin
LC
Aurora Basin
AB
Transantarctic mountains
SW
MDV
EM
Wilkes Basin
BV
EAIS
500 km

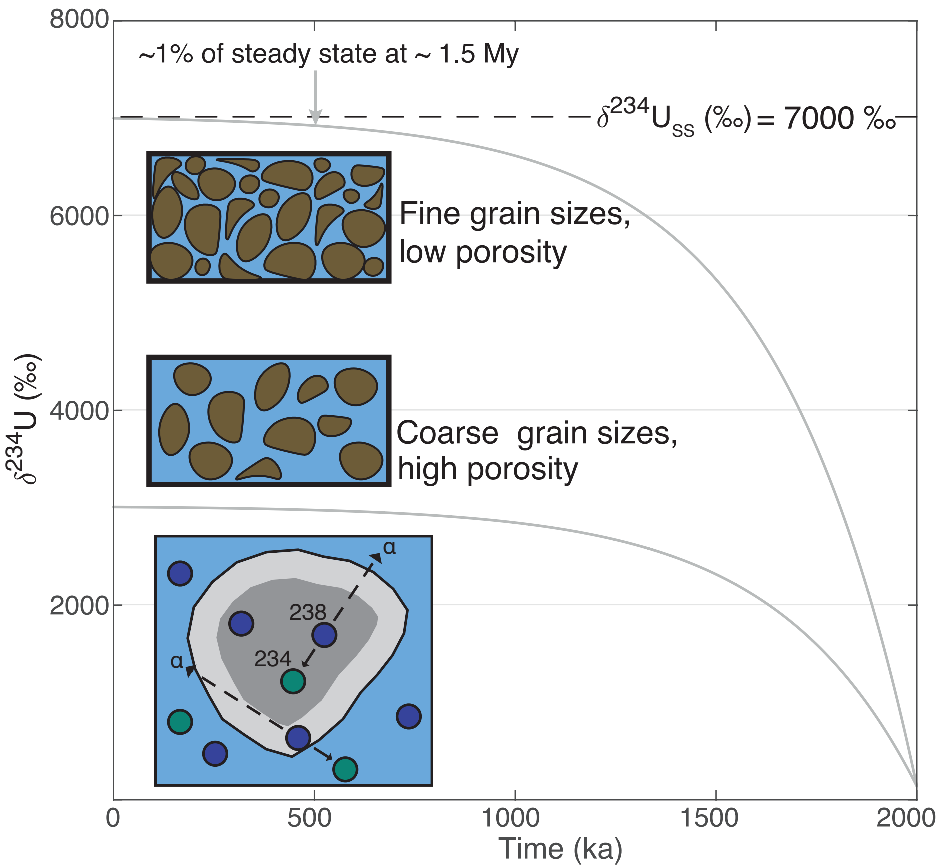

8000
6000
4000
2000
0
500
1000
1500
2000
Time (ka)
$\delta^{234}U$ (‰)
~1% of steady state at ~ 1.5 My
$\delta^{234}U_{SS}$ (‰) = 7000 ‰
Fine grain sizes,
low porosity
Coarse grain sizes,
high porosity
238
234
α
α

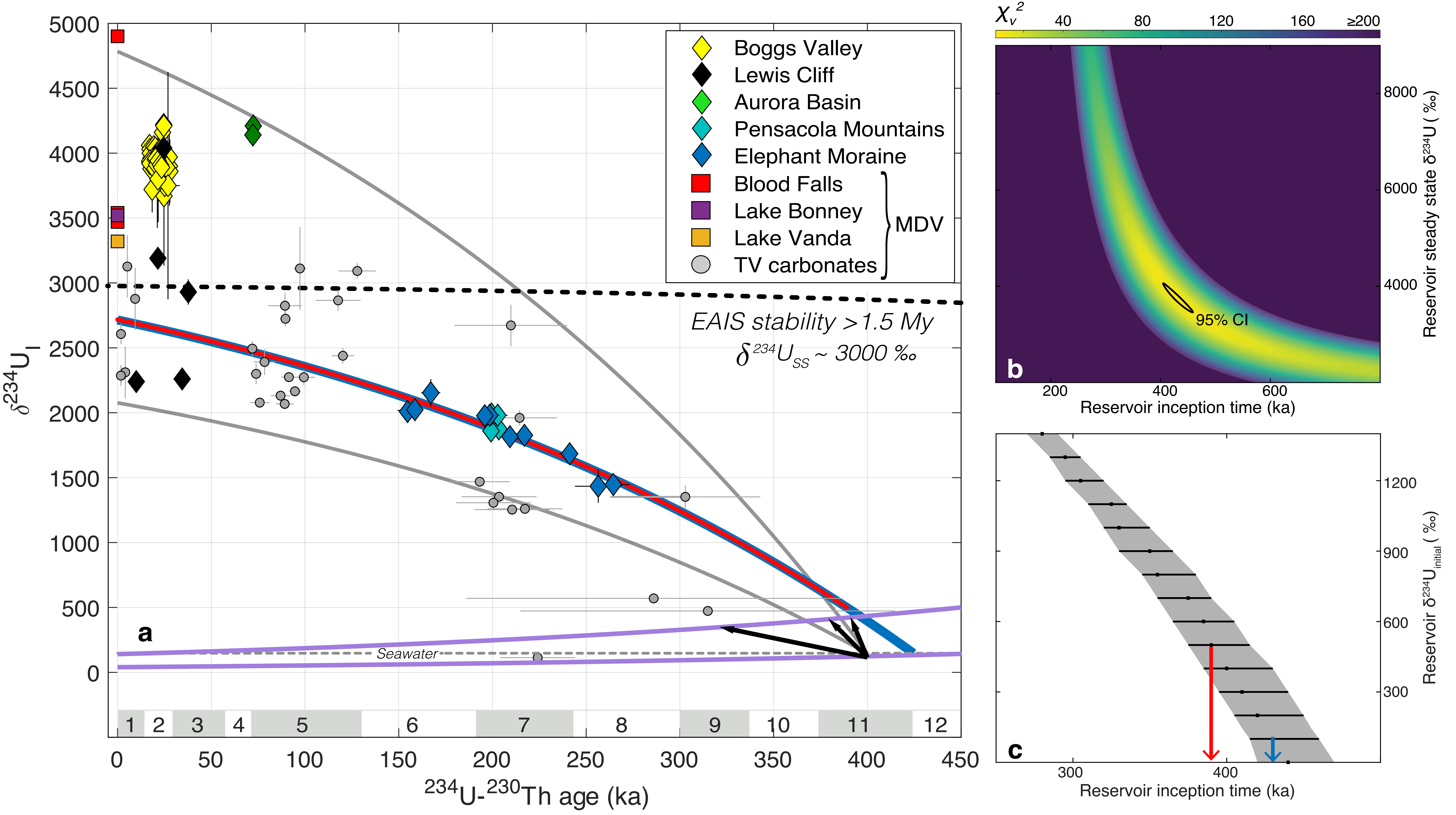

a
b
c
Boggs Valley
Lewis Cliff
Aurora Basin
Pensacola Mountains
Elephant Moraine
Blood Falls
Lake Bonney
Lake Vanda
TV carbonates
MDV
EAIS stability >1.5 My
δ234USS ~ 3000 ‰
Seawater
δ234UI
234U-230Th age (ka)
1 2 3 4 5 6 7 8 9 10 11 12
χν2
40 80 120 160 ≥200
95% CI
Reservoir steady state δ234U (‰)
Reservoir inception time (ka)
Reservoir δ234Uinitial (‰)